

Article

Suitability of Eroded Particles from Die-Sink Electro Discharge Machining for Additive Manufacturing—Review, Characterization and Processing

Oliver Voigt *  and Urs Alexander Peuker 

Institute of Mechanical Process Engineering and Mineral Processing, MVTAT, Technische Universität Bergakademie Freiberg, Agricolastraße 1, 09599 Freiberg, Germany

* Correspondence: oliver.voigt@mvtat.tu-freiberg.de; Tel.: +49-3731-393551

Abstract: In this bipartite study, waste products of die-sink electro discharge machining (die-sink EDM) are investigated. EDM is based on an erosive character of discharges leading to material removal and molten material congeals in the dielectric. The aim is to show a theoretical suitability of these particles for a further usage as a secondary, recycled material in additive manufacturing (AM). Due to the energy- and cost-intensive process of gas atomization for AM powders, there is a need for alternative concepts for particle generation. The first part deals with an intensive review of references from the literature regarding particle size and circularity using image analysis. Secondly, real waste streams were investigated after washing and cleaning processes for oil removal via laser diffraction, dynamic image analysis, SEM with energy dispersive X-ray spectroscopy (EDX) as well as optical emission spectroscopy (ICP OES), categorized within the literature and compared to commercial AM powders. In general, it could be shown that, in principle, recycled particles fulfill main requirements for an AM usage regarding size and shape. Reference powders show median particle sizes of 30 μm to 34 μm and circularities of 0.90 to 0.93, whereas eroded particles exhibit an x_{50} value of 27 μm and circularity of 0.90, too. However, chemical purity, mainly caused by carbon contamination (5.4 wt% in eroded powder compared to 0.4 wt% in reference powder), must be improved before printing via AM machines. Additionally, several separation techniques have to be applied to remove undesired elements (alumina).

Keywords: electro discharge machining; spark erosion; die-sink EDM; wire EDM; EDM debris; additive manufacturing; particle characterization; particle size distribution; recycling



Citation: Voigt, O.; Peuker, U.A. Suitability of Eroded Particles from Die-Sink Electro Discharge Machining for Additive Manufacturing—Review, Characterization and Processing. *Metals* **2022**, *12*, 1447. <https://doi.org/10.3390/met12091447>

Academic Editor: Petru Berce

Received: 28 July 2022

Accepted: 26 August 2022

Published: 30 August 2022

Publisher's Note: MDPI stays neutral with regard to jurisdictional claims in published maps and institutional affiliations.



Copyright: © 2022 by the authors. Licensee MDPI, Basel, Switzerland. This article is an open access article distributed under the terms and conditions of the Creative Commons Attribution (CC BY) license (<https://creativecommons.org/licenses/by/4.0/>).

1. Introduction

Electrical discharge machining (EDM), alternatively spark erosion, is one technique to postprocess components in their shape and texture [1–5], or even to produce metallic and ceramic microspheres [6–9]. In principle, spark erosion techniques are based on an electrical discharge between two electrodes, where a conversion from electrical into thermal energy leads to different mechanisms of material removal in a fluid medium—the so-called dielectric. Historically, this erosive effect was first noted by Joseph Priestley around 1770 [10]. Afterwards two Russian scientists inverted this effect for material removal and invented the first EDM machine [11,12]. In the following years, more and more studies were carried out exploiting this effect for several applications and improving the process to a standard procedure [13–16].

Nowadays, the two dominant techniques are die-sink EDM and wire EDM [17], which are important for several industries, e.g., within mold and vehicle construction for implementing features with high aspect ratios like cavities or slots. It has to be mentioned that the predominantly hard materials have to be electrically conductive. Most of all, several die or hot work steels (martensitic in general) are processed via both technologies, but besides that, other steel types (ferritic, austenitic, etc.) or nickel and aluminum alloys as

well. Main differences are on the one hand the used dielectric fluids and on the other hand the tool electrode geometry as well as the material combination. In die-sink EDM, copper or graphite electrodes are common, whereas in wire EDM a brass or copper wire, which can be partially coated, is used. These processes are performed in synthetic hydrocarbon oil, kerosene in former days (both in die-sink EDM) and deionized water (wire EDM), respectively. Li et al. [18] gave a lucid comparison of these two machining types. Furthermore, some special techniques have been developed, like fast hole drilling EDM [19], micro-EDM [20], near dry EDM [21] or magnetic field/ultrasound assisted EDM [22,23].

In contrast to that, the—compared to EDM—emergent field of additive manufacturing (AM) is becoming more and more important for several industrial sectors and is gaining greater influence and a bigger role every year. Reasons for that are, for example, the very good flexibility, variability and geometrical complexity of producible components. Moreover, a bunch of different materials can be used in a wide range of AM techniques. In the literature, very recommendable reviews can be found that deal with a wide range of usable materials (metals, ceramics, polymers, composite materials, organic/biological material), different AM techniques as well as resulting material properties and specific customized applications [24–28]. In this study, the main focus is on metallic powders only. Some disadvantages are the limitations in manufacturing speed or the post-treatment of the surfaces. Besides that, the AM powders are highly expensive due to their tight specifications regarding particle size distribution (PSD), composition and purity as well as the number of defects accepted. However, these powders should have a narrow particle size distribution (PSD) depending on the manufacturing process. Particles in the size range smaller than 50 μm (median particle size x_{50} around 30 μm) for a selective laser melting (SLM) process or 60 μm to 100 μm (x_{50} around 70 μm to 80 μm , max. particle size around 125 μm) for an electron beam melting (EBM) process, according to [29,30] are commonly used. Moreover, a high circularity/sphericity concerning particle morphology and a low number of defects or hollow particles are required [24]. According to Lui et al., a narrower range of particle sizes leads to better flowability and higher tensile strength and hardness on the one hand, while wider ranges of particle sizes lead to higher powder bed densities, lower laser energy intensities and smoother surface finishes [31]. Apart from that, other important parameters for AM parts are the structure distribution, inherent stress conditions, porosity, laser energy and energy source settings [32,33], respectively.

In Germany, the costs for raw materials in the AM industry for small- and medium-sized enterprises amount to 46% of the total manufacturing costs, according to the Federal Statistical Office [34]. The main reason for that is the production of these specific powders. Right now, there is just the opportunity to generate powders via gas atomization of metal melts [35], which is very energy intensive, too. Therefore, to lower the costs plus energy balance and give, e.g., smaller companies the chance to establish their market presence, an alternative way of supplying and generating metal powders for AM is indispensable.

As a waste product in EDM, so-called erosion sludges or debris, respectively, accumulate. These contain a highly viscous mixture of eroded particles from the two electrodes as well as the oily phase and reaction products from the dielectric. Usually, the debris is led in a filter cartridge or a backflush filter, is filtrated and the dielectric fluid can be used again for several months and years. The disposal of the filters with debris should take place via specialized companies and should follow the waste code AVV 120118, which applies for waste containing mineral oil derivatives in Germany. However, not everyone follows these recommendations; some dispose of mineral oil derivatives in residual waste incorrectly. That has to be considered when looking at the environmental aspects. Yeo et al. [36] reported that, on the one hand, the waste products resulting from the dielectric could be toxic and are not recyclable, and, on the other hand, produced gaseous components can to a minor or major degree be dangerous, such as acetylene, ethylene or hydrogen. Additionally, the electrical energy consumed during the process, mainly in die-sink EDM, cannot be neglected. In a further study, presented by Leão et al. [37], the main source of pollution

was determined in the dielectric fluid with the hydrocarbon oil and the debris, which can cause skin problems or adverse effects to health after inhaling.

Considering the particle sizes as well as the form and circularity of these eroded particles in general, a usage as a secondary material for AM processes should be investigated. Therefore, in this study the first focus lies on an overview of different references dealing with eroded particles in waste material streams from EDM and spark erosion, concerning aspects like size, size distribution, morphology and composition. Secondly, the paper will show an extensive cross-compilation of die-sink EDM sludge and included particles gained from several medium-sized enterprises in middle-east Germany. The results presented should show the theoretical suitability of the particles generated out of these sludges as an alternative, more energy efficient and less expensive AM powder. Concluding, the main focus deals with the particle sizes and forms within the waste streams and not the machining settings or any kind of improvements in the EDM mechanism itself.

2. EDM Eroded Particles

2.1. Particle-Generation Mechanisms

As already mentioned, the main process in EDM is based on an erosive character of generated electrical discharges, caused by the transformation of electrical energy into thermal energy, which leads to a material removal. Therefore, an electrical potential is applied between the two movable/flexible electrodes. The upper electrode is the tool electrode and the lower one the workpiece electrode, which represents the machined component. The dielectric fluid is located in between. The potential leads to the generation of an electrical field and its strength increases until the dielectric strength is exceeded, which leads to the electrical discharge. That discharge takes place at the shortest distance between the electrodes, which is called gap size or spark gap and has a significant influence on the process. As a result, temperature rises in the working zone clearly over 10,000 K, whereby the materials melt. In principle, the whole process is divided into four phases, which are repetitive with a defined frequency adjusted by the pulse generator [17,38]. The first phase contains the impact ionization of the dielectric, where electrons are smashed out of the molecules and form positive ions due to the force of the electric field. Secondly, the phase of ignition follows, dominated by a current flow. The positive ions start to migrate to the workpiece electrode and the negative electrons move to the tool electrode, resulting in a formation of a discharge channel and a temperature and pressure rise. In the third phase, when a constant current flow is reached, the discharge channel expands, plasma is generated and the materials start to melt and vaporize, resulting in a growing cavitation bubble. Finally, in the fourth phase the potential feed is interrupted and the discharge channel collapses. Thereby, the temperature decreases abruptly, the cavitation bubble collapses and the melt vaporizes explosively and carries molten material from deeper areas, which is transported away by the dielectric. Several pulses are repeating in a defined time frame of several micro- or milliseconds until the desired material removal is completed. A schematic sketch of the EDM process is shown in Figure 1.

The eroded particles differ in their size and shape. Dvornik et al. [39] described three characteristic mechanisms for the particle formation. They stated that approx. 10% by volume erode into the vapor phase and the particles are synthesized due to condensation of vaporized material (vaporized particles). This particle fraction is very small (sub- μm or even colloidal), spherical and tends to form agglomerates or attaches on surfaces of bigger particles. A second fraction with 10% by volume, as well, is generated due to brittle failure of the material under the thermal stress and erodes into the solid phase (solid particles). These particles have an irregular shape and differ strongly in their size, which is up to several hundred μm . The majority (about 80 vol.%) erode into the liquid phase due to congealing/solidification of molten metal droplets (molten particles) as well as decreasing of bubbles [40], expulsion of molten material due to bubble explosion of vaporized material or pressure drop [41] at the end of discharge. These generated particles are mostly spherical and the sizes can differ from below 10 μm up to approx. 100 μm . Sizes and ratios of these

three particle generations are strongly influenced by machining conditions. Considering the size ranges and morphology of these three fractions, the particles from the liquid phase are of greatest interest. Vaporized particles are too small for an AM process and stress-cracked particles are too big, irregular in shape and do not show the required sphericity and circularity, respectively. The surface tension forces are responsible for the generation of spherically shaped particles [41–43]. A spherical shape represents the least surface area, which is energetically the best state caused by the time for spheroidization. Thereby, particles tend to form spheres when the time frame is shorter compared to the time for solidification [44–46]. Apart from that, another essential property is the composition of solidified particles, which can significantly change by the formation of several distributed elements in the particle volume, as shown in the literature [39,47–49]. In contrast, vaporized and stress-cracked particles change their phase composition insignificantly. Moreover, an alloying of the eroded particles from the workpiece electrode takes place with material and elements of the tool electrode and dielectric [44,50,51]. In general, spherical particles mostly consist of workpiece material, whereas non-spherical particles consist of tool material. However, there are some major defects observable for a few particles. A lot of them are obtained due to different collision processes of molten droplets and earlier solidified particles. Other common deviations from the spherical shape are particle fusion, cracked or dented surfaces, contaminated surfaces or a satellite formation of smaller particles or agglomerates at the surfaces. The high cooling rate during solidification has a big influence on these factors. Some examples and theories have already been stated in [44,46,52]. Furthermore, a more important problem represents the formation of hollow particles, i.e., hollow spheres. They are caused due to gas entrapments and the charge carriers present in the spark gap [53].

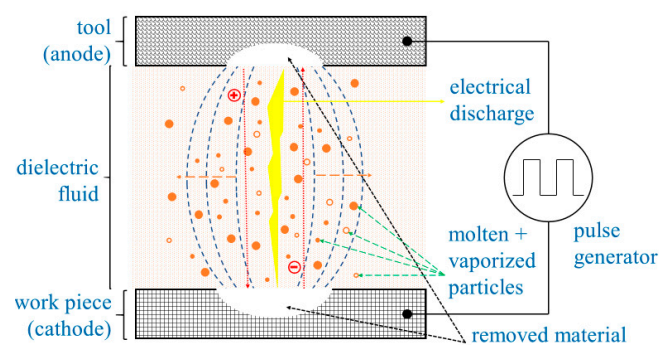


Figure 1. Scheme of electrical discharge mechanism used in EDM. The dotted blue lines represent the phases of the discharge—ionization, ignition, discharge, collapse—red lines the electron and proton migration forming the discharge channel and orange lines the direction of material removal stream.

2.2. Influence of Machining Settings

Commonly used ranges of machining parameters are shown in Table 1, in accordance with the literature [2,5,17,38]. The determining parameters are voltage, discharge current, pulse width/time and gap size. Besides that, the material removal rate (MRR) and tool wear rate (TWR) are two important factors, as well. Hereafter, changes of influencing parameters are shown on size properties, regarding eroded and debris particles, respectively.

Table 1. Characteristic EDM parameter settings.

Parameter	Value
Pulsating voltage	60–300 V
Discharge current	up to 400 A
Pulse frequency	0.2–500 kHz
Pulse width/on time	2 μ s–0.5 ms
Gap size	0.5 μ m–0.5 mm

The first three parameters mentioned in the table above have the most significant influence on particle size and distribution, respectively. For the applied voltage, thus the energy input into the machining area between both electrodes, Khanra et al. [46] stated that the average particle size increases with higher energy values. Furthermore, a higher energy input results in higher currents and pulse lengths as well, which is additionally proven by Katiyar et al. [54]. As a negative side effect, the number of defects also increases, which leads to more dents and cracks on the surfaces due to the higher possibility of collisions among the particles [46,54]. Walter et al. [55] described that the yield of smaller particles decreases with increasing energy and longer time periods. Considering the influence of the chosen discharge current, it goes along with the energy and pulse time. A higher current and longer pulse time leads to higher energy for melting the material, which results in larger-sized particles [52]. In contrast to that, Oßwald et al. [56] could prove smaller particles at a lower discharge current. Furthermore, when applying an increased current at a constant pulse duration, the generated particle sizes increase again, as described by Lin et al. [43]. Khanra et al. confirmed the influence on resulting particle sizes by customizing the pulse time [46]. Longer pulse durations lead to larger particles and shorter ones to smaller particles. This was already reported by Berkowitz et al. [57,58]. In the time period of shorter pulses, more material will be vaporized rather than made molten, which results in smaller particle sizes. Another argument for smaller particles with shorter pulses could be justified by the faster solidification time, as mentioned in [54,56].

One of the most important parameters for the particle composition as well as the size is the choice of the dielectric fluid. Comparing deionized (DI) water with hydrocarbon-based oil, Muttamara et al. [59] described for steels in DI water an oxide formation and generation of the austenitic phase. In contrast to that, machining in oil leads to a carbide formation including development of the martensitic phase with retained austenite, which appears as a dendritic structure. Apart from that, particles eroded in DI water tend to be smaller because water generates a bigger vapor volume in the discharge gap, whereas particles eroded in kerosene/oil became bigger. Some investigations conducted by Leão et al. came to the same results [37]. Moreover, the usage of oil leads to reactions of particles with carbon, hydrogen and oxygen as well as higher carbon and carbide contents due to a pyrolysis of the dielectric [57]. One advantage in using DI is the non-occurrence of contamination in the gap, because no carbon is present, according to Shabgard et al. [60]. As a side effect, discoloration of the fluid can occur, which indicates reaction and oxidization processes within the dielectric itself. Tsukahara et al. reported [61] that metallic particles reacting with this altered oil form organometallic compounds with lipophilic properties. Sanghani et al. [62] offered a detailed review about effects of various dielectrics and powder additives on the machining performance and resulting particle properties. It has to be mentioned that gas can be used as a dielectric, e.g., in near-dry EDM [21], as well.

The MRR und TWR have to be considered as well when discussing the output of debris particles. In general, a higher material removal indicates a higher volume and numbers of eroded particles. It was figured out that MRR and TWR are lower in plain water than in oil [37]. Water has a lower viscosity, which reduces the energy density in the gap and leads to smaller particles and less material removal. In addition, the raised viscosity of a hydrocarbon-based dielectric decreases the MMR due to higher energy densities. Furthermore, decomposing at higher pressures improves the removal rates once more. According to Lin et al. [43], the values for MRR and TWR for cemented tungsten carbide increase with higher discharge currents on the one hand, but decrease with longer pulse duration on the other hand. Li et al. [63] stated that the wear at both electrodes as well as the total machining time are highest in hydrocarbon-based dielectrics. High machining times are induced by thermal decomposition of the dielectric. Singh et al. [64] studied the influence of different electrode materials on the material removal. Thereby, copper and alumina showed the highest material removal.

The gap size represents the discharge length and has to be adapted to the machining conditions. When the gap is increased, a better flushing performance of the dielectric as well

as debris removal are achieved, respectively, as claimed by Prohaszka et al. [65]. Apart from that, the build-up of debris material within the gap, which affects the plasma channel and discharges itself negatively, can be inhibited by varying the gap size to find an acceptable balance between a too short and too long discharge distance [41]. Commonly, the ablated workpiece material solidifies in the dielectric fluid and should be flushed away from this. In contrast to that, Murray et al. [66] observed that machined material could attach on the electrode surface and becomes molten again, which can lead to an undesired debris build-up and inhibition of the flushing process within the gap. This debris migration back to the tool is one discharge gap phenomenon. Within the gap, the flushing performance and removal of the molten and vaporized material is important, which is realized with different flushing modes and electrode geometries [67,68].

In the following, some special cases are listed. Soni et al. [44] found that a higher rotation of the tool electrode in rotary EDM causes smaller particles. Besides that, ultrasonic assistance during the EDM process leads to greater sphericity of the particles, but simultaneously to a larger number of collision dents and defect areas [52]. Last but not least, the addition of specific surfactants inside the dielectric fluid increases the machining efficiency in general, which was discovered by Wu et al. [69]. Another interesting feature caused by a surfactant is more stable and stronger discharge, reducing the particle agglomeration within the debris; this shows a narrower PSD.

3. Comprehensive Overview of Selected Literature

This section of the study shows an overview of different references from the literature, including journal articles, conference papers, lecture books and brochures, regarding different electrode materials, dielectrics, machining parameters and resulting size and shape properties of eroded particles. Table 2 represents a collection and cross comparison of at least 16 references dealing with characteristic material combinations in the field of electro discharge machining and spark erosion, respectively, in the past and present times. Therefore, several tables, PSD and SEM images of these references were exploited. Values out of tables and PSD were adopted in Table 2. To generate quantitative particle size data out of SEM images, the software ImageJ was used by setting a scale bar and measuring the diameters, here the diameter of a circle of equal projection area (EQPC), of depicted particles. Out of these findings the x_{50} /median values, standard deviations and average circularities were calculated and presented with the largest particle size.

Table 2. Overview of debris particle sizes and form factors as well as used parameters.

Reference (year)	Tool Material	Workpiece Material	Dielectric Fluid	Median/ x_{50} and Circularity (–)	Standard Deviation	Largest Particle Size (μm)	Current/Pulse on Time
(1) Tanjilul et al. [70] (2017)	brass	Inconel 718 (Ni-, Cr-based)	synth. oil	≈10.0	–	≈130	48 A/20 μs
				<i>n.s.</i>	–		
				18.1	7.4		
(2) Khanra et al. [46] (2007)	ZrB ₂ -Cu	mild steel	kerosene	0.97	0.07	47	5 μs
				20.7	7.8	56	50 μs
				0.96	0.09		
				23.6	8.1	52	100 μs
				0.95	0.11		
(3) Soni et al. [44] (1994)	Cu-W	die steel	kerosene	12.0	5.0	32	3 A/20 μs
				<i>n.s.</i>	–		
				10.0	3.3	20	9 A/20 μs
				<i>n.s.</i>	–		
				10.0	3.1	20	15 A/20 μs
<i>n.s.</i>	–						

Table 2. Cont.

Reference (year)	Tool Material	Workpiece Material	Dielectric Fluid	Median/ x_{50} (μm) and Circularity (-)	Standard Deviation	Largest Particle Size (μm)	Current/Pulse on Time
(4) Murti et al. [52] (1987) *: with ultrasound assistance	Cu	die steel	kerosene	20.0/24.2 *	6.9/7.9 *	40/45 *	9 A/200 μs
				<i>n.s.</i>	—		
				15.0/19.8 *	6.8/7.6 *	35/40 *	9 A/100 μs
				<i>n.s.</i>	—		
				23.8/32.6 *	7.7/9.3 *	45/65 *	18 A/200 μs
				<i>n.s.</i>	—		
(5) Oßwald et al. [56] (2019)	1.0601 (ferritic steel)	1.0601	synth. oil	20.0/26.2 *	7.2/8.6 *	40/60 *	18 A/100 μs
				<i>n.s.</i>	—		
				35.3	—	\approx 90	52 A/116 μs
				0.94	—		
				13.3	—	\approx 50	39 A/21 μs
(6) Haas et al. [71] (2013)	unknown	unknown	synth. oil	0.91	—		
				11.8	—	\approx 55	17 A/12 μs
				0.90	—		
				89.1	34.0	224	unknown
(7) Walter et al. [58] (1984)	Fe ₇₅ Si ₁₅ B ₁₀	Fe ₇₅ Si ₁₅ B ₁₀	dodecane/Ar (l)	0.89	0.15		
				18.7	2.4	27	unknown
(8) Berkowitz et al. [57] (1987)	Fe ₇₅ Si ₁₅ B ₁₀	Fe ₇₅ Si ₁₅ B ₁₀	dodecane	0.80	0.10		
				11.0	2.2	15	
				<i>n/a</i>	—		
				13.0	3.0	25	25 A/25 μs
				<i>n/a</i>	—		
(9) Rajurkar et al. [72] (1986)	probably AISI 1020	AISI 1020 steel	probably kerosene	13.1	3.5	26	
				<i>n/a</i>	—		
				27.8	3.1	37	
				<i>n/a</i>	—		
				14.2	13.7	—	120 μs
(10) Katiyar et al. [54] (2018)	Cu	die steel	probably synth. oil	<i>n.s.</i>	—		
				18.4	15.9	—	300 μs
				<i>n.s.</i>	—		
				23.0	20.3	—	500 μs
(11) Golubeva et al. [73] (2016)	C-Cu	Ni-20Cr-10Fe-3Ti	mineral oil	<i>n.s.</i>	—		
				7.9	5.3	26	10 A/100 μs
(12) Jutzler/König et al. [17] (1982/2007)	unknown	steel	unknown	0.83	0.25		
				42.6	37.9	189	unknown
(13) Lin et al. [74] (2005)	C	W	kerosene	0.80	0.25		
				22.8	11.9	78	unknown
(14) Storr et al. [38] (2006)	Cu	mixed, die steel	synth. oil	0.62	0.24		
				10.1	6.4	32	15–20 A
(15) Cabanillas et al. [75] (2007)	Fe based alloy	Fe based alloy	kerosene	11.5	6.4	42	unknown
				0.94	0.13		
(16) Ayers et al. [76] (1984)	C	W, Ti, Zr	kerosene	38.0	16.8	92	25 A/30 μs
				<i>n/a</i>	—		
				5.2	3.1	20	\approx 83 μs
				0.88	0.18		

To visualize the range of particles sizes, nine PSDs out of seven references are shown in Figure 2. Two more shown PSDs result from three different machining settings (pulse

on time), which were investigated in that specific study, to show the effects discussed in Section 2.2. Apparently, there is a wide range of material combinations and dielectrics, respectively. Furthermore, different machining settings were used, and sometimes a comparison of changing machining settings was investigated for the same system.

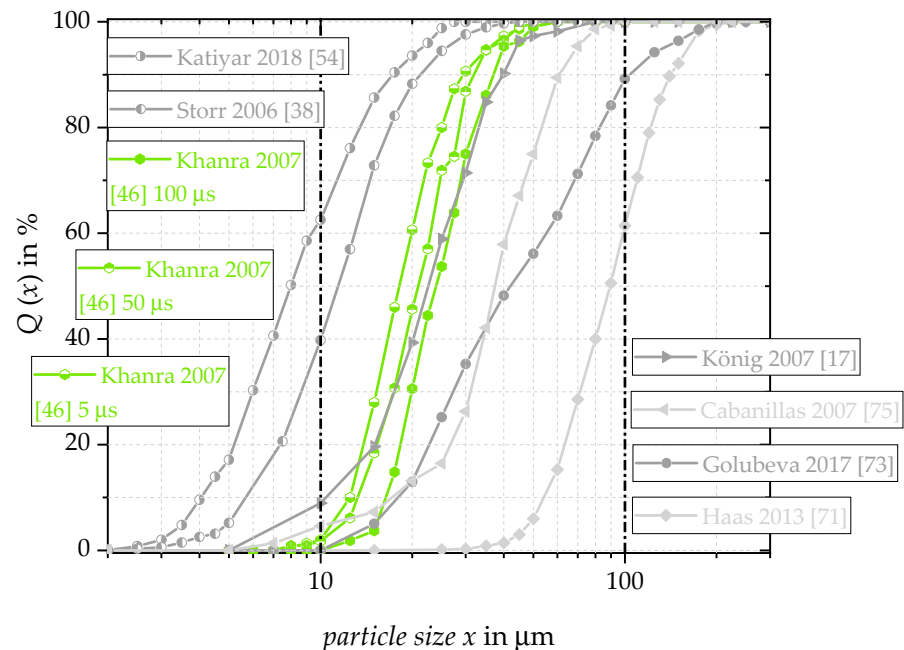


Figure 2. Particle size distributions for selected references gained from ImageJ analysis. Data from [17,38,46,54,71,73,75].

As highlighted in Figure 2, particles from all PSDs presented would be suitable for AM components. The dotted black lines at 10 μm and 100 μm particle size can be defined as borders of AM powder requirements, as mentioned in the introduction. Apart from that, not just the sizes in general, but even the distributions show acceptable results. Thereby, no classifying techniques were applied on these particle systems. Theoretically, by using sieving and/or sifting processes with upper (100 μm to 125 μm) and lower (10 μm to 15 μm) separation cuts, even better results should be achieved. Relatively narrow particle size distributions are observable for nearly all references, which are suitable for an AM process. The x_{50} values and particle sizes indicate a usage for more than one single AM process—techniques from SLM to EBM, direct metal deposition (DMD) or binder jetting are possible. Moreover, the PSDs differ quite strongly, as shown in Katiyar et al. [54], with an x_{50} of around 8 μm for die steel, both machined in synthetic oil, or Haas et al. [71] at around 89 μm for an unknown steel, which represents the highest investigated value as well. It is important to mention that AM powders require an x_{50} values of minimum 20 μm to 25 μm . Taking this into account, the first three and the last reference particles could not be used for further steps without removing the smallest and biggest particles, respectively. Sieving processes would solve this problem and the remaining particles could be used for an AM process. So, for instance, by using an ultra-fine grain sifter for the particle system described in reference (10) [54], the lower separation cut could be set at 15 μm , resulting in a theoretical usage of the upper approx. 35% of the particles. The remaining particles below 15 μm are suitable for a binder jetting process, etc. In addition to that, nearly all particles in reference (2) [46] fit well to AM requirements and could be used further in an SLM process. Moreover, considering the PSD obtained from (6) [71] nearly 30% to 40% of the particles, which are larger than 125 μm , are not useable in AM and should be removed with a sieve. For a handful of cases, some partitions between an SLM or EBM technique should be made. Sieving processes would result in—minimum—two size fractions, whereby each fraction is

suitable for one AM technique. This would make sense in the case of analyzed references (11) [73] or (15) [75].

Smallest particle sizes were obtained by Ayers et al. [76] for tungsten machined in kerosene with around five microns. In general, it is quite conspicuous that a lot of the smallest particle sizes were reported when machining tungsten and tungsten-based alloys and materials [39,60], with the aim of producing metal carbides [6]. Quite a few analyzed circularity values do not meet the specifications for an AM powder. The minimum value for circularity should be 0.85, whereby a value of 1 represents the ideal circle. The best results were obtained for references (2) [46] and (5) [56], combined with their x_{50} values; the particle systems fit nearly completely to requirements for further applications. Bad examples are shown for references (8) [57] and (13) [74], whereby the image quality and brightness as well as the contrast ratios led to unsatisfactory results, even though acceptable particle shapes are visible.

4. Materials and Methods

Filter cartridges from die-sink EDM machines were collected from regional companies and were sent to the research facility. The amount of delivered cartridges or sludges differs quite strongly for each company and these are registered simultaneously to obtain an impression of accumulating waste. Thereby, the operating time of a cartridge can be very high, meaning that some companies can provide several cartridges per year, which would be around some kilograms of waste, whereas others produce significantly higher kg amounts. Additionally, cartridges operate until a defined time period of machining hours is exceeded or until reaching a pressure indication. Furthermore, raw sludge can be collected in small containers. Information about geometries, masses and used materials of received sample cartridges is stated in Table 3, and representative images are given in Figure 3. It has to be mentioned that no information about processing/machining parameters for the sludge containing cartridges is available. The implemented software in these used EDM machines automatically adjusts parameters for current, voltage, pulse width and gap size according to the component, depending on geometry, desired shape or material.

Table 3. Overview of investigated filter cartridges.

Filter Cartridge	Dielectric Fluid	Tool Material	EDM Machine	Dimensions $d \times h$ [cm] & Mass [kg]	Yield of Sludge [kg]
(1) SE_01-MT die-sink	synthetic hydrocarbon oil	99.9% graphite	OPS-Ingersoll Eagle 800	30.5×50.5 $m = 17.09$ (wet)	3.95 (wet)
(2) SE_02-AP die-sink	synthetic hydrocarbon oil	99.9% graphite	GF Machining Solutions	15.0×35.5 $m = 5.19$ (wet)	0.46 (wet)

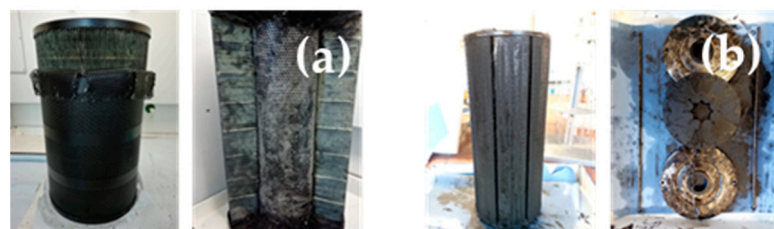


Figure 3. Investigated filter cartridges, left: (a) SE_01-MT, right: (b) SE_02-AP.

To extract the sludges/debris, a dismantling step was necessary due to the design of the cartridges (Figure 4). The black and oily sludge was enclosed in a metallic cylinder with a perforated mesh. With the help of some tools, it was possible to remove these parts and to uncover filter material and slats, which collect the sludge after the flushing mechanism to reuse the dielectric. Finally, the material from the nonwoven fabric was scraped off and

collected. In Figure 3, all steps of dismantling are shown. For another filter type, the filter material without any shell was delivered. In general, sludge consists of three different components, which are the oily phase, particles from the tool electrode—graphite—and particles from the workpiece electrode—always metallic particles.



Figure 4. Flow sheet of dismantling, extraction of waste debris/sludge, example for SE_01.

After filtration, the particles were washed again in acetone and/or isopropanol and finally dried in an oven overnight at 80 °C. As a side effect of the filtration processes, effects of sedimentation behavior were investigated. With time, the heavier steel particles settled at the bottom of the flasks and the supernatant solution containing the lighter particles and most of the graphite was decanted, resulting in two different fractions of particles for further characterization, which were mostly graphitic flakes of the filter cake on the paper, and metallic residues in the glass flasks.

Measurements with laser diffraction, permanently with cuvette R3, and with dynamic image analysis in 300 mL liquid with a stirrer at 600 rpm and pump speed at 65 rpm (HELOS and QICPIC LIXELL, both Sympatec GmbH, Clausthal-Zellerfeld, Germany) were carried out to quantify particle size and shape, especially circularity, in a dry or wet (dispersed in isopropanol and/or DI water) state. The initial sludge could be suspended in isopropanol with ultrasound assistance (3 min, 50% amplitude, cycle 1) and was measured with laser diffraction as well to compare size values before and after filtration and cleaning procedures. All of the following investigations were performed with cleaned and processed particles and fractions. An upper separation cut was introduced with sieves of a mesh size of 125 µm.

Apart from that, images were taken via a desktop SEM (with 10 kV, Phenom, FEI/Thermo Fisher Scientific Inc., Waltham, MA, USA) with BSE imaging (through backscattered electrons) to achieve additional size and shape information as well as typical particle defects like cracks, dents and satellites. For an impression of the chemical composition of eroded particles, investigations with another SEM in BSE mode (with 10 kV or 20 kV, XL30 ESEM FEG, FEI/Thermo Fisher Scientific Inc., Waltham, MA, USA) combined with energy-dispersive X-ray spectroscopy (Software EDAX Genesis, Ametek Inc., Berwyn, IL, USA) were conducted on sputtered samples.

Afterwards, a new standard for optical emission spectroscopy with inductively coupled plasma (ICP OES; iCAP 6300, Thermo Fisher Scientific Inc., Waltham, MA, USA) could be calibrated containing elements out of EDX results of typical alloy elements. These were Al, Co, Cr, Cu, Fe, Mn, Mo, Ni, P, Si and V. The standard solutions were obtained from Carl Roth (GmbH and Co. KG, Karlsruhe, Germany). Before measuring, samples were dissolved and boiled in aqua regia. The sample masses differ between 100 mg and 300 mg. The carbon and sulfur content was measured using a G4 Icarus C-S-Analyzer (Bruker AXS GmbH, Karlsruhe, Germany). Thereby, around 1 g of sample material was combusted in an oxygen stream and measured with two infrared detectors each for C and S after calibrating the device with certified steel reference materials.

Hereafter, thermogravimetric analysis (TGA) via differential scanning calorimetry (DSC; STA 443 F3 Jupiter, Netzsch GmbH and Co. KG, Selb, Germany) was performed for oil containing samples SE_01-MT and SE_02-AP in a nitrogen atmosphere from room temperature up to 1000 °C with a heat rate of 10 K min^{−1}.

To compare results of eroded particles, two reference materials were chosen and investigated with exactly the same methods. Reference materials were steel powder of austenitic stainless steel 316L/1.4404/X2CrNiMo17-12-3 (Hoeganaes Corporation, Starck

Surface Technology and Ceramic Powders GmbH, Goslar, Germany) with a particle size range of 15 μm to 45 μm (max. 5% over-/undersize) and martensitic hot work steel H11/1.2343/X37CrMoV5-1 (GKN Powder Metallurgy/GKN Hoeganaes Corporation Europe, Buzau, Romania) with a range of 15 μm to 53 μm , respectively, according to data sheets. The reasons for choosing these two specific powders are explained in Section 5.3 regarding the results of the analysis of their chemical composition.

5. Results and Discussion

5.1. Comparison of Literature Values, Real Waste Streams and AM Reference Materials

In Figure 5, the analyzed x_{50} values of 13 particle systems out of eight representative literature references, which were generated with different machining settings, are plotted against their circularity values and compared to each other as well as to reference materials and eroded particles, respectively. Dotted vertical lines represent the upper and lower median particle sizes for AM processes and the horizontal line indicates the minimum value for their circularity. The abbreviation ‘Set X’ indicates a specific machining setting within the same material system of the particular literature and ‘AM Ref’ a commercial reference material used in AM. Particle systems showing low circularity values are not presented in Figure 5 due to their lack of suitability, but are displayed in Table 3. Moreover, some particle systems show a big scattering within their circularity values as well as their x_{50} values. Overall, it can be stated that the eroded particles extracted from SE_01 (cyan star) already fit well with the requirements with an x_{50} close to 30 μm and a circularity of 0.9. By removing agglomerates from the SE_01 sample, visible in dynamic image analysis, which results from attachments of several smaller spherical particles, the values for circularity can even be increased. With sieving and sifting, the median particle size of this sample can be optimized.

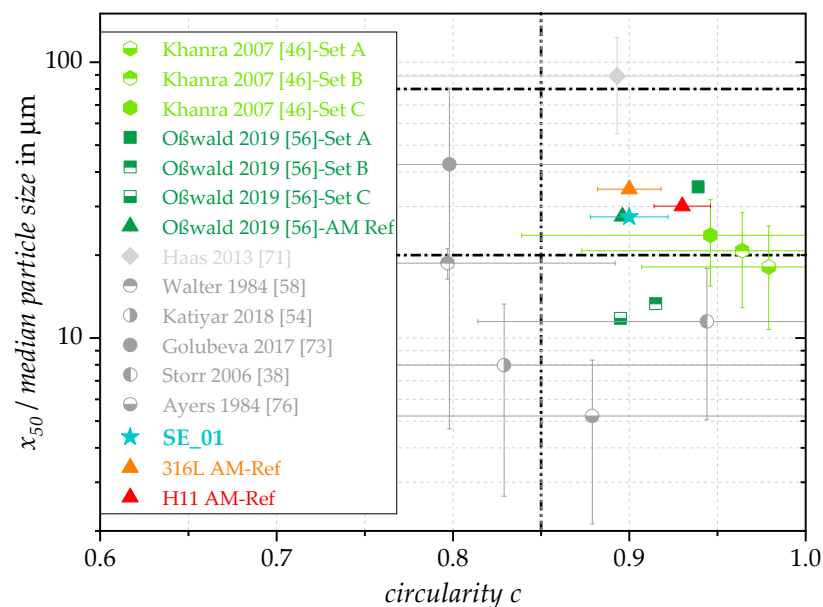


Figure 5. $x_{50,3}$ values against circularity values for 13 particle systems out of the literature compared to AM reference materials (316L/1.4404 + H11/1.2343) and die-sink EDM waste (SE_01). Data from [38,46,54,56,58,71,73,76].

Comparing SE_01 with eroded particles from Golubeva et. al. [73], who tried a printing process of components in an SLM machine, SE_01 shows better properties. Their results were not acceptable because printed parts collapsed and were not stable enough. Maybe the PSD was not optimized; thus, there is no detailed information given, just a very narrow range of 30 μm to 50 μm . Besides that, from image analysis it is conspicuous that the circularity is definitely not high enough at below 0.8 and it scatters as well, whereas the x_{50}

value is ok, maybe a little too high. Moreover, Oßwald et al. [56] reported one machined fraction, which fits very well with the requirements. Two others with different machining settings have too small median particle sizes, which should be optimized by processing steps, but have good circularities. References [54,58] cannot fulfill any requirement, thus representing unsuitable waste streams, whereas references [38,71] and maybe [76] fulfill requirements regarding their circularities. With additional processing steps, x_{50} values can be shifted to desired sizes.

Looking at the performance of eroded particles compared to both acquired commercial AM materials, sample SE_01 is already on a very good level. The data points are very close together, just with a little bit lower x_{50} value, but even equally high circularity, which is underlined in Figure 6, too. The green triangle is an AM reference as well, and overlaps nearly perfectly with our investigated recycled powder. In fractions resulting from different machining settings shown in [46,56], very good results for circularities are achieved. Only median particle sizes have to be adjusted. It can be concluded that several eroded particle systems fulfill the main requirements and should be considered for a direct recycling chain.

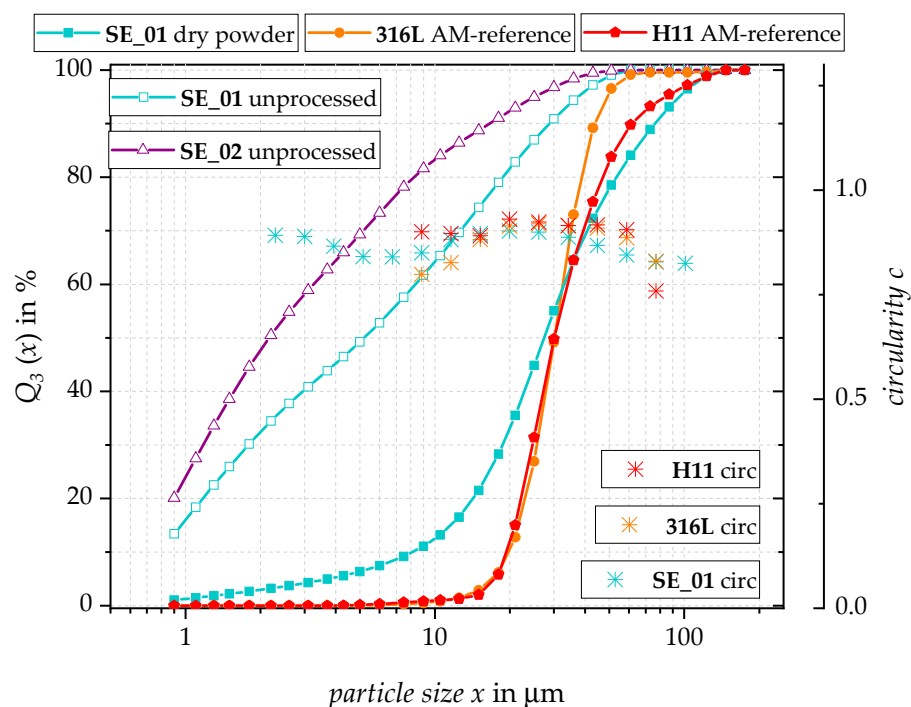


Figure 6. Particle size distributions of unprocessed sludges SE_01-MT and SE_02-AP, processed and dry particles of SE_01-MT as well as commercial AM powder 316L/1.4404 and H11/1.2343.

5.2. Particle Size Distributions and Particle Morphologies

Figure 6 illustrates different PSDs as well as circularities for both die-sink EDM sludges (unfilled), processed eroded particles of SE_01 and both reference materials (filled). Circularities are shown as single data points. In Table 3, the characteristic particle values are outlined.

The size distribution of both sludges is obviously bimodal and has a very wide range of particle sizes. Svedberg already claimed in 1924 that a bimodal PSD could be a consequence of an oscillatory arc [42], as it is used in EDM. Already 13% (SE_01) or even up to 20% (SE_02) of all particles are $0.9 \mu\text{m}$ or smaller, which is the technical limit of the used cuvette. By looking at the targeted minimum particle size for the chosen AM processes of $10 \mu\text{m}$ to $15 \mu\text{m}$, it is quite underwhelming for SE_02 that only approx. 15% of the particles could be used in further processes. In contrast to that, for SE_01, nearly 40% could be recycled. These results are comparable to investigations from Walter et al. [55] or Berkowitz et al. [57], who found for their particle system that up to 70% of the particles are smaller than $20 \mu\text{m}$.

Compared to Golubeva et al. [73], where only 15% of the particles are in a suitable size range, particles from SE_01 show better results. It is not clear which material from which electrode is present in each size class. Due to thermal stresses and vaporization effects, amounts of graphitic electrode material could accrue in the smallest and largest size classes, whereas the congealed material from the steel electrode tends to erode more into liquid than into vapor due to its ductile behavior [39] resulting in bigger particles from the liquid phase. Besides that, graphite particles distinguish clearly from metal particles, as seen in Figures 7 and 8. Their shapes are irregular and differ strongly, whereas metallic particles tend to form spheres with high circularity. However, circularities cannot be measured with certainty for small particle sizes, since the resolution limit in a dynamic image analysis device is reached below $5\ \mu\text{m}$ to $10\ \mu\text{m}$.

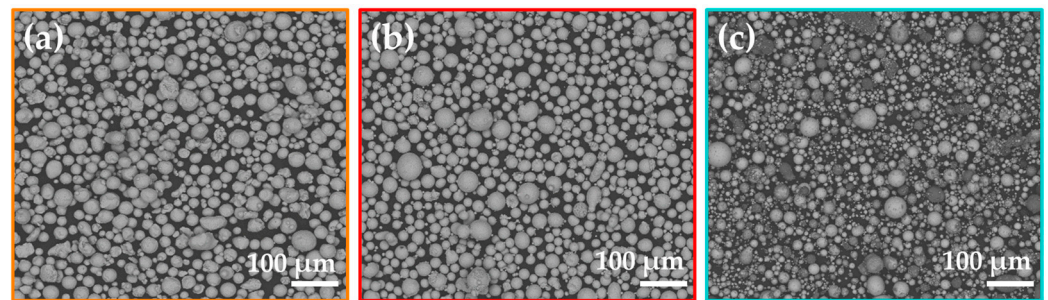


Figure 7. SEM images of commercial reference materials in AM: (a) 316L, (b) H11/1.2343, (c) eroded particles from SE_01-MT.

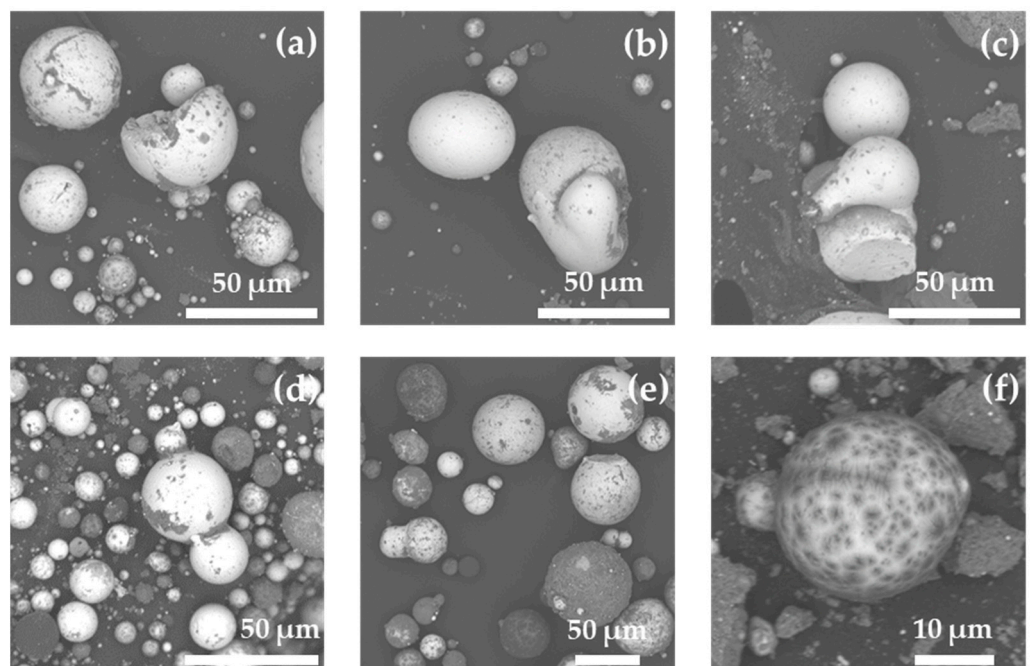


Figure 8. SEM images showing typical particle defects: (a) agglomerates, gas entrapments and cracks, (b) particle fusion, (c) dents, splats, platelets, (d) satellites and particle fusion, (e) particle collision and fusion, strong surface contamination, (f) dendritic structure (+brittle graphite fragments).

For processed, dried and sieved SE_01 particles, a lower separation cut is visible. Compared to raw sludge, approx. 1% instead of 65% are below $10\ \mu\text{m}$. The x_{50} value shifted from $5.21\ \mu\text{m}$ to $27.52\ \mu\text{m}$ and is close to the references with $34.66\ \mu\text{m}$ and $30.08\ \mu\text{m}$, respectively. Besides that, the PSD is not as narrow as it should be for a secondary usage, as can be seen in the x_{10} and x_{90} values. Therefore, additional sieving and sifting processes

are suggested to create at least two or three fractions. However, the x_{90} value for the H11 reference is relatively high with 61.68 μm , compared to the 316L reference. With an ultra-fine grain sifter, the lower separation cut will be optimized. Afterwards, sieving with a 45 μm or 63 μm sieve to obtain a fraction for SLM processes (approx. 60%) should be carried out. The remaining 30% of the particles up to 125 μm are suitable for EBM processes. Particles below 15 μm to 20 μm can be considered for a usage in binder jetting.

Both reference materials show a narrow and normally distributed PSD, as could be assumed. Their particle sizes differ between approx. 10 μm and 60 μm . Circularity values (in Table 4) are on a high and mostly constant level of around 0.9, but decrease slightly with an increase in the particle size, maybe caused by the optical resolution. For the smallest particles, a downshift in circularities is observed, too. This trend is noticeable for eroded particles, as well. However, the H11 reference has the highest circularity with 0.93, whereas the chemically related SE_01 powder and different reference 316L show both values of 0.90, which fulfills the requirements for AM powders as well, combined with the overall good x_{50} values. Upper and lower cuts for SE_01 must be improved in further steps via sieving and sifting.

Table 4. x_{50} and circularity values for die-sink EDM particles and both AM reference materials.

Sample/Value	SE_01 Unprocessed	SE_02 Unprocessed	SE_01 Dry Powder	316L/1.4404 Reference	H11/1.2343 Reference
x_{10} (μm)	0.80	0.70	8.15	22.89	19.37
x_{50} (μm)	5.21	2.16	27.52	34.66	30.08
x_{90} (μm)	28.89	16.61	76.60	49.23	61.68
circularity	—	—	0.90	0.90	0.93

Information about the masses of oil and solid phase, which is split up into graphitic and metallic parts roughly, was gained via filtration and washing experiments as well as TGA-DSC analysis. Sludge SE_01 shows an oil content of around 55 wt% to 60 wt%, whereas SE_02 contains significantly more oil with around 85 wt%. By means of filtration and decanting, the solid contents of SE_01 could be roughly separated from each other and have amounts of approx. 15 wt% for metallic residues in the flasks and around 20 wt% to 25 wt% of graphitic flakes with metallic inclusions. It is important to mention that it was not possible to gain enough metallic material out of cartridge SE_02-AP. The very high oil content and very high amount of extremely small particle sizes, as seen in Figure 6 (PSD), was quite challenging. Besides that, the amount of sludge in these filter cartridges is very low in general; it would not be useful or profitable enough to consider this specific waste stream for further usage; see Table 3. Therefore, no measurements with laser diffraction and dynamic image analysis of dry powder could be performed.

SEM images in Figure 7 show morphological properties of both commercial reference AM powders (a + b) and the processed particles of SE_01 (c). What was already seen in the PSD and associated Table 4 can be confirmed. All three particle systems have a quite similar size range, though for SE_01 some very small as well as sometimes big particles are present, since this is the virgin material without further processing. For both reference powders, typical defects like satellites or particle fusion are visible, though not in that low amount compared to eroded particles. Thereby, nearly all particles show very constant circular shapes. However, for some particles, strong surface contaminations, resulting in rougher surfaces, are visible; their origin is investigated and explained in Section 5.3 via EDX analysis. Besides that, due to the ordinal number/material contrast, a mixture of brighter and darker particles is observable (also demonstrated in Figure 9b), whereas brighter ones are present in larger numbers. Darker particles can be distinguished between surface contaminated brighter ones and regular darker ones consisting of second metallic material caused by machining of two sufficiently different metallic components in the same device.

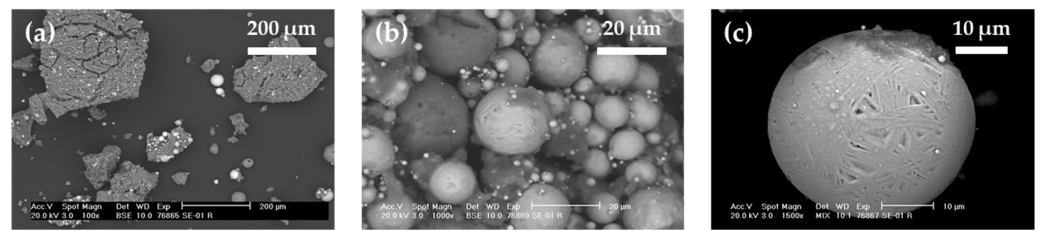


Figure 9. SEM images of SE_01-MT sample used for EDX analysis: (a) graphite particles with enclosed metallic spheres, (b) spherical debris of steel and aluminum alloy with lots of (sub-micron) agglomerates, (c) spherical particle with carbon contamination on surface, lamellar structure.

Overall, the morphologies of all metal powders look quite good. Particles show good spherical shapes and a low number of defects, which could be confirmed by the measurements applying dynamical image analysis (Table 4). The surfaces appear relatively smooth. Measurements with atomic force microscopy (AFM) may confirm these assumptions in the future by comparing the surface roughness values of all the particle systems regarding the influence of the different cooling speeds and temperature gradients during resolidification. Moreover, reference powders appear to have a higher number of satellites, which is due to the atomization process.

However, there are some typical defects observable in eroded particles as well, which are collected in Figure 8. It is quite common that some particles show irregular shapes and anomalies in their shape, structure or surface. Khanra et al. [46] and Murti et al. [52] discussed typical particle defects in erosion sludges, which are comparable to the ones presented here. All defects are shown for commercial AM powders in the literature [29,77,78] as well, and can also be confirmed in Figure 7a,b. The number of these defects should always be low and in an acceptable range, which can be correlated with circularity values or circularity distributions, respectively. Particles with low circularities will have some defects like particle fusion, agglomeration, gas entrapments, dents, splats or cracks. Other typical observations are dendritic structures of surface contaminations. Latter ones should definitely be removed or minimized, which will be achieved with a secondary cleaning and washing step and/or ultrasonic assistance during oil removal.

5.3. Chemical Composition

At first, an EDX analysis of SE_01 was performed to obtain an impression about machined metallic components. Some characteristic areas, which were analyzed via the x-ray beam, are shown in Figure 9. Sometimes, metallic particles are enclosed in or agglomerated around graphitic fragments, which are caused by thermal stresses and induced brittle failure (Figure 9a). In Figure 9b, a mixture of brighter and darker particles is present—brighter ones are detected as steel particles and darker ones as alumina (partially oxidized) particles. The amount of alumina particles is significantly lower. Surface contaminations are observable again (e.g., Figure 9c) and could be identified as carbon structures originating from the pyrolysis of the dielectric fluid and/or the graphitic electrode. Mainly, the results indicate a machining of two different metallic components, which should be separated from each other in an additional processing step, for example, by magnetic or density separation (susceptibility and density values differ sufficiently). In the following, Al particles are not considered further due to their low amount and the high oxygen peaks in their EDX spectra. The iron-based eroded particles are assignable to a typical alloy, which is mainly used in the sector of mold and vehicle construction, namely H11, 1.2343 or X37CrMoV5-1. Considering these results, the choice of reference materials was unequivocal. To compare properties of eroded particles, commercial AM powder for SLM machines of martensitic hot work steel H11/1.2343 was chosen. Additionally, a second and most commonly used AM material in laser powder bed fusion and the automotive sector was investigated to have another comparison with industrial products. This is stainless steel 316L, 1.4404 or X2CrNiMo17-12-3, which shows a different magnetic behavior due to the

austenitic microstructure [79]. For both reference powders, PSDs and SEM images are shown above (Figures 6 and 7a,b) and chemical compositions in Table 5 below.

Table 5. Results of ICP OES and C-S-Analyzer for filter cakes of SE_01 + SE_02 without oil (1 + 2), SE_01 dry powder (3), commercial AM powder H11/1.2343 (4) and target values (5).

	Al (wt%)	Co (wt%)	Cr (wt%)	Cu (wt%)	Mn (wt%)	Mo (wt%)	Ni (wt%)	P (wt%)	Si (wt%)	V (wt%)	C (wt%)	S (wt%)
(1)	26.88	0.53	4.34	0.57	0.65	1.04	1.13	0.06	0.46	0.33	n.a.	n.a.
(2)	—	—	3.79	0.98	0.93	0.60	1.51	0.14	0.77	0.27	n.a.	n.a.
(3)	5.75	0.52	4.31	0.19	0.41	1.21	1.14	0.04	0.42	0.38	5.40	0.013
(4)	—	—	4.79	0.02	0.60	1.36	0.09	0.012	1.40	0.44	0.40	0.005
(5)	—	—	4.50–5.50	—	0.20–0.60	1.10–1.60	—	0.03	0.60–1.25	0.25–0.60	0.33–0.43	≤0.03

The chemical compositions of several samples of eroded particles (1–3) and reference material H11 (4) are shown in Table 5. Thereby, for SE_01, one should distinguish between two fractions resulting from the cleaning/washing steps. These are silver-grey metallic residues (3) and black-graphitic flakes with metallic inclusions (1) out of the filtration process. The content of iron always maintains the remaining balance.

A comparison of SE_01 (1) with SE_02 (2) shows nearly the same composition of hot-work steel H11/1.2343, without any side elements in SE_02. After queries with the companies, H11/1.2343 was confirmed. It is interesting to observe the untypical amount of Al, Ni and Co in SE_01 samples, which results from a different alloy resulting from machined Al-based materials with typical alloying elements Ni and Co, including an amount of Cu. When comparing the metallic residue (3) with the filter cake (1), in residues a significantly higher iron amount in balance is observable. By contrast, the Al amount in filter cake structures is about five times bigger. This results from the step of decanting and the high difference in the density values, which distinguish between 7.8 g cm^{-3} for steel particles, 2.7 g cm^{-3} for Al particles and 2.2 g cm^{-3} for remaining graphite particles. High amounts of Fe-based particles as well as bigger/heavier Al and graphite particles in the suspension settle down, whereas lighter ones, mostly Al and graphite, but also very small Fe-based particles, are decanted and filtrated. Besides that, the values for Si and Cr are a little bit too low, but overall the alloy composition is sufficient enough.

Results from the C-S-Analyzer confirm the assumptions of a higher carbon content after machining due to alloying effects from the graphite electrode as well as a pyrolysis of the hydrocarbon-based dielectric. Values for C in data sheets are given with 0.33 wt% to 0.43 wt%, whereas around 5.4 wt% C was investigated for eroded particles of SE_01, which is stated and comparable to another study with 4.69 wt% [56]. To decrease the carbon content to an acceptable range, several options may be possible. On the one hand, the contaminated surfaces can be cleaned properly to remove excessive carbon, which can be achieved via an energy input by an ultrasound sonotrode and/or by stressing the particles in a (wet grinding) ball mill without additional grinding balls to expose the particles to mutual shear processes and shear forces due to particle collision and induce a cleaning effect. On the other hand, via density separation techniques, excessive carbon between the particles in each size class could be removed simultaneously with Al particles. A certain amount of carbon cannot be resolved because, due to diffusion processes during the melting and congealing phases, an increased irreversible migration of carbon atoms into the crystal lattice of iron can be expected.

The amount of sulfur is in an acceptable range. In datasheets, a maximum is given with about 0.02 wt.% to 0.03 wt% max., whereas eroded particles show a value of approx. 0.013 wt%. However, the chemical purity in general must be improved.

6. Conclusions and Outlook

In this study, the principle suitability of eroded particles originating from electro discharge machining after processing and cleaning steps could be shown. By investigating several literature references using image analysis software and evaluating SEM images

as well as particle size distributions given in these articles, a theoretical suitability of eroded particles was underlined. After processing the sludges via cleaning, washing, filtrating, decanting in organic solvents and classifying, characterizations of these particles were performed regarding the important specifications such as particles size distribution, morphology, circularity as well as chemical composition. The particle sizes (distribution) of eroded particles already fits quite well with those of the references by looking at the x_{50} values, but they are not as narrow as they should be; this can be customized by sieving and sifting processes. The circularities are overall on a high level and comparable with commercial materials.

Further steps will be implemented in following studies to enhance the quality of the recycled powders to improve their suitability as a secondary AM material and, finally, to investigate their performance in AM processes comparing to chosen reference materials. Additionally, the chemical purity must be improved. Sieving and sifting processes will be performed to create two or three size fractions. To separate the Al particles and remaining graphite particles from the steel particles, different physical separation characteristics will be considered. Other characterization methods of powder samples will be carried out to obtain further detailed information about the particle systems, e.g., bulk solid mechanics. By using reference materials, parameter settings in AM machines will be found and optimized, followed by the production of different specimens and investigations of them via several mechanical tests. Moreover, upper and lower rejects from processing could be used in further AM techniques and it is worth considering a secondary usage of graphitic residues in different applications as well. In the near future, a focus on wire-EDM machines, which operate in hydrocarbon oil as well, may be conceivable.

Author Contributions: Conceptualization, O.V. and U.A.P.; methodology, O.V.; validation, O.V. and U.A.P.; formal analysis, O.V.; investigation, O.V.; data curation, O.V.; writing—original draft preparation, O.V.; writing—review and editing, U.A.P.; visualization, O.V.; supervision, U.A.P.; project administration, U.A.P. and O.V.; funding acquisition, U.A.P. All authors have read and agreed to the published version of the manuscript.

Funding: This research was funded by the German research association DECHEMA Society for Chemical Engineering and Biotechnology e.V., grant number IGF 21692 BR, and the Federal Ministry for Economic Affairs and Climate Protection on basis of a resolution of the German Bundestag.

Data Availability Statement: The data presented in this study are available on request from the corresponding author.

Acknowledgments: The authors thank the technicians of the MVTAT institute for their support, Annett Kästner for measurements of particle size distributions and Yvonne Völkner (both TUBAF/MVTAT) for conducting the ICP OES measurements. In addition, the authors thank the companies for providing the investigated filter cartridges, Gert Schmidt for performing SEM-EDX-analysis and Thilo Kreschel (both TUBAF, IKFVW and IEST) for measuring samples in C-S-analyzer.

Conflicts of Interest: The authors declare no conflict of interest.

References

1. Petrofes, N.F.; Gadalla, A.M. Electrical discharge machining of advanced ceramics. *Am. Ceram. Soc. Bull.* **1988**, *67*, 1048–1052.
2. Ho, K.H.; Newman, S.T. State of the art electrical discharge machining (EDM). *Int. J. Mach. Tools Manuf.* **2003**, *43*, 1287–1300. [[CrossRef](#)]
3. Guu, Y.H.; Hocheng, H.; Chou, C.Y.; Deng, C.S. Effect of electrical discharge machining on surface characteristics and machining damage of AISI D2 tool steel. *Mater. Sci. Eng. A* **2003**, *358*, 37–43. [[CrossRef](#)]
4. Schumacher, B.M. After 60 years of EDM the discharge process remains still disputed. *J. Mater. Processing Technol.* **2004**, *149*, 376–381. [[CrossRef](#)]
5. Mohd Abbas, N.; Solomon, D.G.; Fuad Bahari, M. A review on current research trends in electrical discharge machining (EDM). *Int. J. Mach. Tools Manuf.* **2007**, *47*, 1214–1228. [[CrossRef](#)]
6. Ayers, J.D. Initiation of ZrC Dendritic Growth on the Surface of Spark Machined Zirconium. *Metall. Trans. A* **1983**, *14*, 5–10. [[CrossRef](#)]
7. Sato, T.; Usuki, K.; Okuwaki, A.; Goto, Y. Synthesis of metal nitrides and carbide powders by a spark discharge method in liquid media. *J. Mater. Sci.* **1992**, *27*, 3879–3882. [[CrossRef](#)]

8. Kocova, M.; Pizurova, N.; Süllow, S.; Schneeweiss, O. Composition and tempering of Fe-C and Fe-Ni-C fine particles prepared by spark erosion. *Mater. Sci. Eng. A* **1995**, *190*, 259–265. [[CrossRef](#)]
9. Cabanillas, E.D.; López, M.; Pasqualini, E.E.; Cirilo Lombardo, D.J. Production of uranium–molybdenum particles by spark-erosion. *J. Nucl. Mater.* **2004**, *324*, 1–5. [[CrossRef](#)]
10. Schumacher, B.M.; Krampitz, R.; Kruth, J.P. Historical Phases of EDM Development Driven by the Dual Influence of “Market Pull” and “Science Push”. *Procedia CIRP* **2013**, *6*, 5–12. [[CrossRef](#)]
11. Lazarenko, B.R. *About the Inversion of Metal Erosion and Methods to Fight Ravage of Electric Contacts*; WEI-Ins: Moscou, Russia, 1943.
12. Lazarenko, B.R.; Lazarenko, N.I. *Physics of the Spark Method of Machining Metals*; TsBTI MÉP: Moscow, Russia, 1946.
13. Solotykh, B.N. *Fundamental Physics of Electroerosion on Metals*; Physics-Mathematical Library (Gostekhisdat): Moscou, Russia, 1953.
14. Zolotykh, B. The mechanism of electrical erosion of metals in liquid dielectric media. *Soviet Phys. Tech. Phys.* **1959**, *4*, 1370.
15. Bucklow, I.; Cole, M. Spark-machining. *Metall. Rev.* **1969**, *14*, 103–118. [[CrossRef](#)]
16. Lunina, M.A.; Novozhil, Y.A. Electrical condensation method for preparation of metal dispersions in organic media. *Colloid J. Ussr* **1969**, *31*, 370.
17. König, W.; Klocke, F. *Fertigungsverfahren: Abtragen, Gnerieren und Lasermaterialbearbeitung*; Springer: Berlin/Heidelberg, Germany, 2007; Volume 4, p. 412.
18. Li, L.; Li, Z.Y.; Wei, X.T.; Cheng, X. Machining Characteristics of Inconel 718 by Sinking-EDM and Wire-EDM. *Mater. Manuf. Processes* **2014**, *30*, 968–973. [[CrossRef](#)]
19. Yilmaz, O.; Okka, M.A. Effect of single and multi-channel electrodes application on EDM fast hole drilling performance. *Int. J. Adv. Manuf. Technol.* **2010**, *51*, 185–194. [[CrossRef](#)]
20. Schubert, A.; Zeidler, H.; Hahn, M.; Hackert-Oschätzchen, M.; Schneider, J. Micro-EDM Milling of Electrically Nonconducting Zirconia Ceramics. *Procedia CIRP* **2013**, *6*, 297–302. [[CrossRef](#)]
21. Gholipour, A.; Baseri, H.; Shabgard, M.R. Investigation of near dry EDM compared with wet and dry EDM processes. *J. Mech. Sci. Technol.* **2015**, *29*, 2213–2218. [[CrossRef](#)]
22. Singh Bains, P.; Sidhu, S.S.; Payal, H.S. Investigation of magnetic field-assisted EDM of composites. *Mater. Manuf. Processes* **2017**, *33*, 670–675. [[CrossRef](#)]
23. Nani, V.-M. The ultrasound effect on technological parameters for increase in performances of W-EDM machines. *Int. J. Adv. Manuf. Technol.* **2016**, *88*, 519–528. [[CrossRef](#)]
24. DebRoy, T.; Wei, H.L.; Zuback, J.S.; Mukherjee, T.; Elmer, J.W.; Milewski, J.O.; Beese, A.M.; Wilson-Heid, A.; De, A.; Zhang, W. Additive manufacturing of metallic components—Process, structure and properties. *Prog. Mater. Sci.* **2018**, *92*, 112–224. [[CrossRef](#)]
25. Ngo, T.D.; Kashani, A.; Imbalzano, G.; Nguyen, K.T.Q.; Hui, D. Additive manufacturing (3D printing): A review of materials, methods, applications and challenges. *Compos. Part B Eng.* **2018**, *143*, 172–196. [[CrossRef](#)]
26. Gu, D.D.; Meiners, W.; Wissenbach, K.; Poprawe, R. Laser additive manufacturing of metallic components: Materials, processes and mechanisms. *Int. Mater. Rev.* **2013**, *57*, 133–164. [[CrossRef](#)]
27. Bourell, D.; Kruth, J.P.; Leu, M.; Levy, G.; Rosen, D.; Beese, A.M.; Clare, A. Materials for additive manufacturing. *CIRP Ann.* **2017**, *66*, 659–681. [[CrossRef](#)]
28. Singh, S.; Ramakrishna, S.; Singh, R. Material issues in additive manufacturing: A review. *J. Manuf. Processes* **2017**, *25*, 185–200. [[CrossRef](#)]
29. Strondl, A.; Lyckfeldt, O.; Brodin, H.; Ackelid, U. Characterization and Control of Powder Properties for Additive Manufacturing. *Jom* **2015**, *67*, 549–554. [[CrossRef](#)]
30. Kruth, J.P.; Froyen, L.; Van Vaerenbergh, J.; Mercelis, P.; Rombouts, M.; Lauwers, B. Selective laser melting of iron-based powder. *J. Mater. Process. Technol.* **2004**, *149*, 616–622. [[CrossRef](#)]
31. Liu, B.; Wildman, R.; Tuck, C.; Ashcroft, I.; Hague, R. Investigation The Effect of Particle Size Distribution on Processing Parameters Optimisation In Selective Laser Melting Process. In Proceedings of the 22nd Annual International Solid Freeform Fabrication Symposium—An Additive Manufacturing Conference, Online, 2–4 August 2021; pp. 227–238.
32. Brandl, E.; Leyens, C.; Palm, F. Mechanical Properties of Additive Manufactured Ti-6Al-4V Using Wire and Powder Based Processes. In *Proceedings of the IOP Conference Series Materials Science and Engineering*; IOP Publishing: Bristol, UK, 2011; Volume 26. [[CrossRef](#)]
33. Munsch, M.; Schmidt-Lehr, M.; Wycisk, E. Metal Additive Manufacturing with sinter-based technologies. In *AM Power Insights*; AMPOWER: Hamburg, Germany, 2018.
34. Statistisches Bundesamt, Kleine und Mittlere Unternehmen. 2020. Available online: https://www.destatis.de/DE/Themen/Branchen-Unternehmen/Unternehmen/Kleine-Unternehmen-Mittlere-Unternehmen/_inhalt.html (accessed on 12 July 2021).
35. Tsunekawa, Y.; Ueno, T.; Okumiya, M.; Yashiro, T. Plasma Sprayed Coatings with Water and Gas Atomised Bearing Steel Powders. *Surf. Eng.* **2013**, *19*, 17–22. [[CrossRef](#)]
36. Yeo, S.H.; Tan, H.C.; New, A.K. Assessment of waste streams in electric-discharge machining for environmental impact analysis. *Proc. Inst. Mech. Eng. Part B* **1998**, *212*, 393–401. [[CrossRef](#)]
37. Leão, F.N.; Pashby, I.R. A review on the use of environmentally-friendly dielectric fluids in electrical discharge machining. *J. Mater. Processing Technol.* **2004**, *149*, 341–346. [[CrossRef](#)]
38. Storr, M. Wissenswertes zur Senkerosion. In *Oelheld GmbH—Innovative Fluid Technology*; Oelheld GmbH: Stuttgart, Germany, 2006; Volume 1, pp. 1–44.

39. Dvornik, M.I. Nanostructured WC–Co particles produced by carbonization of spark eroded powder: Synthesis and characterization. *Int. J. Refract. Met. Hard Mater.* **2010**, *28*, 523–528. [[CrossRef](#)]
40. Lu, X.; Pan, Y.; Liu, K.; Liu, M.; Zhang, H. Spark model of pulsed discharge in water. *J. Appl. Phys.* **2002**, *91*, 24–31. [[CrossRef](#)]
41. Murray, J.W.; Sun, J.; Patil, D.V.; Wood, T.A.; Clare, A.T. Physical and electrical characteristics of EDM debris. *J. Mater. Process. Technol.* **2016**, *229*, 54–60. [[CrossRef](#)]
42. Svedberg, T. *Colloid Chemistry: Wisconsin Lectures*; Chemical Catalog Company, Inc. Book Department: New York, NY, USA, 1924; Volume 16.
43. Lin, Y.-C.; Chen, Y.-F.; Lin, C.-T.; Tzeng, H.-J. Electrical Discharge Machining (EDM) Characteristics Associated with Electrical Discharge Energy on Machining of Cemented Tungsten Carbide. *Mater. Manuf. Processes* **2008**, *23*, 391–399. [[CrossRef](#)]
44. Soni, J.S. Microanalysis of debris formed during rotary EDM of titanium alloy (Ti 6Al 4V) and die steel (T 215 Cr12). *Wear* **1994**, *177*, 71–79. [[CrossRef](#)]
45. Davila, L.P.; Leppert, V.J.; Risbud, S.H. Microstructure and microchemistry of silicon particles formed during electrical-discharge machining. *J. Mater. Sci. Mater. Electron.* **2003**, *14*, 507–510. [[CrossRef](#)]
46. Khanra, A.K.; Pathak, L.C.; Godkhindi, M.M. Microanalysis of debris formed during electrical discharge machining (EDM). *J. Mater. Sci.* **2007**, *42*, 872–877. [[CrossRef](#)]
47. Berkowitz, A.; Walter, J.; Wall, K. Magnetic properties of amorphous particles produced by spark erosion. *Phys. Rev. Lett.* **1981**, *46*, 1484. [[CrossRef](#)]
48. Berkowitz, A.E.; Walter, J.L. Amorphous Particles Produced by Spark Erosion. *Mater. Sci. Eng.* **1982**, *55*, 275–287. [[CrossRef](#)]
49. Berkowitz, A.; Hansen, M.F.; Parker, F.; Vecchio, K.; Spada, F.; Lavernia, E.; Rodriguez, R. Amorphous soft magnetic particles produced by spark erosion. *J. Magn. Magn. Mater.* **2003**, *254*, 1–6. [[CrossRef](#)]
50. Soni, J.S. Experimental investigation on migration of material during EDM of die steel (T215 Cr12). *J. Mater. Processing Technol.* **1996**, *56*, 439–451. [[CrossRef](#)]
51. Gill, A.S.; Kumar, S. Surface alloying of H11 die steel by tungsten using EDM process. *Int. J. Adv. Manuf. Technol.* **2015**, *78*, 1585–1593. [[CrossRef](#)]
52. Murti, V.S.R.; Philip, P.K. An analysis of the debris in ultrasonic-assisted electrical discharge machining. *Wear* **1987**, *117*, 241–250. [[CrossRef](#)]
53. Holmgren, J.; Gibson, J.; Sheer, C. *Ultrafine Particles*; Wiley: New York, NY, USA, 1963.
54. Katiyar, J.K.; Sharma, A.K.; Pandey, B. Synthesis of iron-copper alloy using electrical discharge machining. *Mater. Manuf. Processes* **2018**, *33*, 1531–1538. [[CrossRef](#)]
55. Walter, J.L. Preparation of Powder by Spark Erosion. *Powder Metall.* **1988**, *31*, 267–272. [[CrossRef](#)]
56. Oßwald, K.; Woidasky, J.; Hoffmann, A.M.; Moser, M. Suitability of electrical discharge machining debris particles for usage as a powder for selective laser melting: An explorative study. *Prog. Addit. Manuf.* **2019**, *4*, 443–449. [[CrossRef](#)]
57. Berkowitz, A.E.; Walter, J.L. Spark erosion: A method for producing rapidly quenched fine powders. *J. Mater. Res.* **1987**, *2*, 277–288. [[CrossRef](#)]
58. Walter, J.L.; Berkowitz, A.E. Effect of Cooling Rate on the Atomic and Crystal Structure of Rapidly Cooled Fe75Si15B10. *Mater. Sci. Eng.* **1984**, *67*, 169–177. [[CrossRef](#)]
59. Muttamara, A.; Kanchanomai, C. Effect of Carbon in the Dielectric Fluid and Workpieces on the Characteristics of Recast Layers Machined by Electrical Discharge Machining. *Metall. Mater. Trans. A* **2016**, *47*, 3248–3255. [[CrossRef](#)]
60. Shabgard, M.R.; Kabirinia, F. Effect of Dielectric Liquid on Characteristics of WC-Co Powder Synthesized Using EDM Process. *Mater. Manuf. Processes* **2014**, *29*, 1269–1276. [[CrossRef](#)]
61. Tsukahara, H.; Minami, H.; Hagino, H.; Lee, S.; Masui, K.; Sone, T. EDM Using Chemical Reaction of Organometallic Compounds. *Int. J. Electr. Mach.* **2007**, *12*, 29–34.
62. Sanghani, C.R.; Acharya, G.D. Effect of Various Dielectric Fluids on Performance of EDM: A Review. *Trends Mech. Eng. Technol.* **2016**, *6*, 55–71.
63. Li, C.; Xu, X.; Li, Y.; Tong, H.; Ding, S.; Kong, Q.; Zhao, L.; Ding, J. Effects of dielectric fluids on surface integrity for the recast layer in high speed EDM drilling of nickel alloy. *J. Alloys Compd.* **2019**, *783*, 95–102. [[CrossRef](#)]
64. Singh, S.; Maheshwari, S.; Pandey, P.C. Some investigations into the electric discharge machining of hardened tool steel using different electrode materials. *J. Mater. Process. Technol.* **2004**, *149*, 272–277. [[CrossRef](#)]
65. Prohaszka, J.; Mamalis, A.G.; Vaxevanidis, N.M. The effect of electrode material on machinability in wire electro-discharge machining. *J. Mater. Process. Technol.* **1997**, *69*, 233–237. [[CrossRef](#)]
66. Murray, J.; Zdebski, D.; Clare, A.T. Workpiece debris deposition on tool electrodes and secondary discharge phenomena in micro-EDM. *J. Mater. Process. Technol.* **2012**, *212*, 1537–1547. [[CrossRef](#)]
67. Li, L.; Gu, L.; Xi, X.; Zhao, W. Influence of flushing on performance of EDM with bunched electrode. *Int. J. Adv. Manuf. Technol.* **2011**, *58*, 187–194. [[CrossRef](#)]
68. Goigana, M.; Elkaseer, A. Self-Flushing in EDM Drilling of Ti6Al4V Using Rotating Shaped Electrodes. *Materials* **2019**, *12*, 989. [[CrossRef](#)]
69. Wu, K.L.; Yan, B.H.; Lee, J.-W.; Ding, C.G. Study on the characteristics of electrical discharge machining using dielectric with surfactant. *J. Mater. Process. Technol.* **2009**, *209*, 3783–3789. [[CrossRef](#)]

70. Tanjilul, M.; Ahmed, A.; Kumar, A.S.; Rahman, M. A study on EDM debris particle size and flushing mechanism for efficient debris removal in EDM-drilling of Inconel 718. *J. Mater. Process. Technol.* **2017**, *255*, 263–274. [[CrossRef](#)]
71. Haas, P.; Pontelandolfo, P.; Perez, R. Particle Hydrodynamics of the Electrical Discharge Machining Process. Part 1: Physical Considerations and Wire EDM Process Improvement. *Procedia CIRP* **2013**, *6*, 41–46. [[CrossRef](#)]
72. Rajurkar, K.P.; Pandit, S.M. Formation and Ejection of EDM Debris. *J. Eng. Ind.* **1986**, *108*, 22–26. [[CrossRef](#)]
73. Golubeva, A.A.; Sotov, A.V.; Agapovichev, A.V.; Smelov, V.G.; Dmitriev, V.N. Research of the possibility of using an electrical discharge machining metal powder in selective laser melting. *Mater. Sci. Eng.* **2017**, *177*, 012119. [[CrossRef](#)]
74. Lin, M.-H. Synthesis of nanophase tungsten carbide by electrical discharge machining. *Ceram. Int.* **2005**, *31*, 1109–1115. [[CrossRef](#)]
75. Cabanillas, E.D. TEM observations of particles obtained by electro-erosion in kerosene. *J. Mater. Sci.* **2007**, *42*, 3155–3160. [[CrossRef](#)]
76. Ayers, J.D.; Moore, K. Formation of Metal Carbide Powder by Spark Machining of Reactive Metals. *Metall. Trans. A* **1984**, *15*, 1117–1127. [[CrossRef](#)]
77. Farzadfar, S.A.; Murtagh, M.J.; Venugopal, N. Impact of IN718 bimodal powder size distribution on the performance and productivity of laser powder bed fusion additive manufacturing process. *Powder Technol.* **2020**, *375*, 60–80. [[CrossRef](#)]
78. Niu, H.J.; Chang, I.T.H. Selective laser sintering of gas and water atomized high speed steel powders. *Scr. Mater.* **1999**, *41*, 25–30. [[CrossRef](#)]
79. Mumtaz, K.; Takahashi, S.; Echigoya, J.; Kamada, Y.; Zhang, L.; Kikuchi, H.; Ara, K.; Sato, M. Magnetic measurements of the reverse martensite to austenite transformation in a rolled austenitic stainless steel. *J. Mater. Sci.* **2004**, *39*, 1997–2010. [[CrossRef](#)]